

Probing the Rashba effect via the induced magnetization around a Kondo impurity

R. Chirla,^{1,*} C. P. Moca,^{1,2} and I. Weymann³

¹*Department of Physics, University of Oradea, 410087, Oradea, Romania*

²*BME-MTA Exotic Quantum Phase Group, Institute of Physics, Budapest University of Technology and Economics, H-1521, Budapest, Hungary*

³*Faculty of Physics, Adam Mickiewicz University, 61-614, Poznań, Poland*

(Received 10 April 2013; published 27 June 2013)

When a single magnetic adatom is deposited on a surface of a metal, it affects the charge and spin texture of the electron gas surrounding it. The screening of the local moment by conduction electrons gives rise to the Kondo effect. Here we investigate the effect of the Rashba spin-orbit coupling on the local magnetization density of states (LMDOS) around a Cobalt impurity on an Au(111) surface in a magnetic field. We show that the in-plane component of the LMDOS is exclusively associated with the Rashba spin-orbit interaction. This observation can be experimentally exploited to confirm the presence of the Rashba effect on surfaces, such as Au(111), by performing spin-polarized scanning tunneling microscopy measurements around the Kondo impurity.

DOI: [10.1103/PhysRevB.87.245133](https://doi.org/10.1103/PhysRevB.87.245133)

PACS number(s): 72.15.Qm, 72.25.-b, 75.70.Tj

I. INTRODUCTION

In two-dimensional structures, the coupling between the spin and angular momentum can lead to a variety of interesting phenomena.¹ Interestingly enough, the Rashba spin-orbit (SO) interaction² has become one of the intriguing and desired ingredients of modern nanoelectronics and spintronics.³ Studying the Rashba-induced effects for atoms placed on surfaces is especially interesting because, on one hand, it opens up a way to probe the strength of the SO coupling, and on the other hand, it may allow one to explore the interplay between the Kondo screening and the SO interaction. In this regard, the Au(111) surface is very promising since it exhibits a measurable energy splitting of surface band states, which was first experimentally observed by LaShell *et al.*⁴ However, because the Friedel oscillations induced by an adatom remain practically unaffected by the Rashba SO interaction,⁵ the presence of the Rashba effect could not be verified by typical scanning tunneling microscopy (STM) measurements, focused mainly on the charge transport spectroscopy. Measurable local electron density changes do appear in the case of quantum corrals.^{6,7} Also, the Rashba effect of a two-dimensional (2D) gas created by Cs atoms on *p*-type InSb(110) has been experimentally quantified by STM, where it shows up as a beating pattern as a function of applied voltage.⁸ The influence of the SO interaction on the Kondo physics was also studied in C nanotubes.⁹ It has been noticed only very recently that placing a magnetic adatom on the surface can help probe the Rashba spin-orbit effect. By treating the impurity at the classical level and in the absence of the Kondo effect, Lounis *et al.*¹⁰ have shown that the induced spin polarization of the electron gas surrounding the magnetic adatom exhibits a spin texture, which is a superposition of two skyrmionic waves with opposite chirality. This has been attributed to the presence of the Rashba SO interaction.

In the present work we pursue this problem further and study the local texture of the spin-resolved density of states around the magnetic adatom in the case of nontrivial many-body interactions, such as the ones leading to the Kondo effect,¹¹ and in the presence of an external magnetic field applied along the *z*th direction. The Kondo effect, which occurs

when a local impurity spin in a metallic host is screened by the conduction electrons, is undoubtedly one of the fundamental effects in condensed matter physics.¹² It has been shown that the Kondo effect survives in the presence of SO interaction.¹³ It was later predicted that the Rashba coupling will change the Kondo temperature through a modification of the effective bandwidth,¹⁴ and this analysis was continued by others.^{15–18}

Here we investigate how the induced local magnetization density of states (LMDOS) around a magnetic adatom in the Kondo regime, in the presence of an external magnetic field, is affected by the Rashba SO interaction.

In the many body formalism, the LMDOS, $\mathbf{M}(\mathbf{r}, E)$, can be expressed in terms of the retarded, single-particle Green's function, $\mathcal{G}(\mathbf{r}, \mathbf{r}', E)$, as

$$\mathbf{M}(\mathbf{r}, E) = -\frac{1}{\pi} \text{Im} \text{Tr}_{\sigma} \{ \boldsymbol{\sigma} \mathcal{G}(\mathbf{r}, \mathbf{r}, E) \}, \quad (1)$$

where $\boldsymbol{\sigma}$ are the Pauli matrices, E is the energy measured with respect to the Fermi energy E_F , and \mathbf{r} is the in-plane distance from the impurity. The real-space Green's function $\mathcal{G}(\mathbf{r}, \mathbf{r}, E)$ shall be computed in terms of the many-body \mathcal{T} matrix for the conduction electrons, which describes the scattering of the surface electrons off the impurity.

To make quantitative estimates, we focus on a Co atom on an Au(111) surface,^{19,20} for which a Kondo temperature T_K of about 75 K was extracted from STM spectroscopy measurements.²⁰ The Au(111) surface is modeled within the tight binding approximation (TBA), which, in spite of its simplicity, is able to properly describe the dispersion of the Au surface states.²¹ To capture the Kondo physics correctly, the Co impurity is described in terms of the Anderson model.²² The many-body \mathcal{T} matrix is related to the Green's function describing the local orbitals of the Co ion (see Sec. II B 2), which can be then computed with the aid of the numerical renormalization group (NRG) method,²³ known as the most versatile and accurate in treating quantum impurity problems. Moreover, to make realistic predictions, in NRG calculations we take into account the full energy dependence of the density of states (DOS) of the Au(111) surface. While in general the magnetic impurity itself can have a complicated orbital

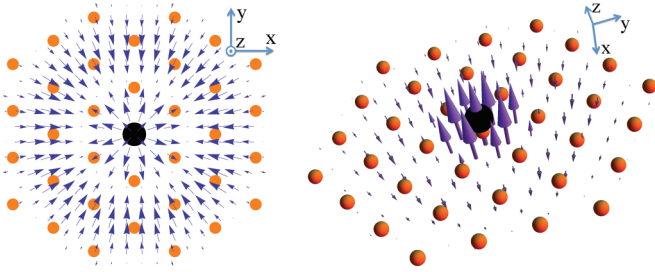


FIG. 1. (Color online) Spatial distribution of the radial component \mathbf{M}_r (left panel) and of the total LMDOS \mathbf{M} (right panel) at energy $E = -2$ meV below the Fermi surface, and for a magnetic field $B = 3$ T applied along the z th direction. The smaller (orange) spheres indicate the position of the Au atoms on the Au(111) surface, and the large (black) sphere represents the magnetic adatom. The arrows indicate the amplitude and direction of the LMDOS.

structure, and channels with different symmetries may couple to the surface, within the NRG approach the coupling is assumed to have an s -wave symmetry.

One of the main results of this paper—a nonvanishing in-plane magnetization \mathbf{M}_r —is sketched in Fig. 1 together with the total magnetization \mathbf{M} in a magnetic field, $B = 3$ T. Notice that at $B = 0$, the local polarization vanishes, $\mathbf{M} = 0$. Although the total LMDOS $\mathbf{M} = (M_x, M_y, M_z)$ is an important quantity, we have found that the in-plane component \mathbf{M}_r is much more interesting, as it is strongly affected by the presence of the SO interaction. On the other hand, the out-of-plane part, M_z , depends weakly on the Rashba interaction and displays a spatial behavior that is somewhat similar to the one observed in the local density of states (LDOS).^{19,24–26} More than that, \mathbf{M}_r is a pure Rashba effect, as it vanishes if the SO interaction is turned off.

Experimentally, it is possible to measure the radial component of the energy-dependent LMDOS with the state-of-the-art spin-polarized STM techniques,²⁷ which can thus provide an important information on the presence and strength of the Rashba SO interaction. In this paper, using realistic parameters, we study the behavior of the energy and position-dependent LMDOS in the region around the magnetic impurity.

The paper is organized as follows. In Sec. II we introduce our model Hamiltonian that describes the Au surface. The description of the magnetic impurity problem is also presented in the same section. In Sec. III we present and discuss our numerical results. We close with conclusions in Sec. IV, where our main findings are reiterated.

II. THEORETICAL FRAMEWORK

A. Modeling the Au(111) surface

Let us introduce the details of the lattice under investigation, the tight-binding Hamiltonian describing it, and the corresponding band structure. The Au(111) surface presents a hexagonal structure, with one atom per unit cell. The basis vectors of the direct lattice are $\mathbf{t}_1 = (\sqrt{3}/2, 1/2)a$ and $\mathbf{t}_2 = (-\sqrt{3}/2, 1/2)a$, with a the lattice constant ($a = 5.75$ Å). Here we are particularly interested in the changes induced locally by a magnetic impurity in the LMDOS. We shall

not address the so-called herringbone reconstruction,²⁸ which may be relevant when analyzing photoemission spectra. Also, the external magnetic field is assumed to produce no kinetic effects on the surface states, as its effect is marginal. In spite of its simplicity, this tight binding description is rather robust, and can be checked against more sophisticated *ab initio* band structure calculations,²⁹ or compared to experimentally measured binding energies.⁴

1. Hamiltonian for the Au(111) surface

We model the Au(111) surface in terms of a tight binding Hamiltonian,²¹ taking into account the hopping between the nearest-neighbor p_z orbitals subject to the Rashba SO interaction

$$H_0 = \sum_{(\mathbf{r}, \mathbf{r}')} \sum_{\sigma} (t_{\mathbf{r}, \mathbf{r}'} + E_p \delta_{\mathbf{r}, \mathbf{r}'}) \Psi_{\mathbf{r}, \sigma}^{\dagger} \Psi_{\mathbf{r}', \sigma} + i\alpha \sum_{(\mathbf{r}, \mathbf{r}')} \sum_{\sigma \sigma'} \left[\boldsymbol{\sigma} \times \frac{\mathbf{r} - \mathbf{r}'}{|\mathbf{r} - \mathbf{r}'|} \right]_{\sigma \sigma'}^z \Psi_{\mathbf{r}, \sigma}^{\dagger} \Psi_{\mathbf{r}', \sigma'}. \quad (2)$$

The first term describes the hopping and the on-site energies, while the second one is due to the Rashba spin-orbit coupling. Here, $\Psi_{\mathbf{r}, \sigma}^{\dagger}$ creates an electron in the Au p_z orbital at position \mathbf{r} with spin σ , $t_{\mathbf{r}, \mathbf{r}'}$ are the nearest-neighbor hoppings between these orbitals, and E_p denotes their on-site energies. In the second term, α is the strength of the Rashba interaction.

By fitting the tight binding dispersion, $\varepsilon_{\tau}(\mathbf{k})$, to the experimentally measured binding energy of Ref. 4 along the $\bar{\Gamma}\bar{M}$ direction, one can extract the band parameters:²¹ $t = -0.30$ eV, $E_p = 1.41$ eV, and $\alpha = 0.02$ eV. We note that the effect of the external magnetic field on the surface electrons is rather minimal. A simple analysis of the energies involved shows that the Zeeman splitting for a magnetic field of about 3 T (the g factor was taken to be $g = 2.5$) is $\Delta E_Z = 0.43$ meV, i.e., five times smaller than the Rashba energy: $E_R = -3\alpha^2/(2t) = 2.08$ meV, and tiny as compared to the band parameters t and E_p . Consequently, the effect of the magnetic field on the conduction electrons is neglected.

The Hamiltonian (2) can be diagonalized in Fourier space by expanding the field operators $\Psi_{\mathbf{r}, \sigma}$ as

$$\Psi_{\mathbf{r}, \sigma} = \frac{1}{\sqrt{\Omega}} \sum_{\mathbf{k}, \tau} e^{i\mathbf{k}\cdot\mathbf{r}} e_{\tau, \sigma}(\mathbf{k}) c_{\mathbf{k}, \tau}, \quad (3)$$

where Ω is the number of unit cells, and $c_{\mathbf{k}, \tau}$ annihilates an electron with momentum \mathbf{k} in the chiral band $\tau = \pm 1$. Then, the dispersion is $\varepsilon_{\tau}(\mathbf{k}) = E_p + G(\mathbf{k}) + \tau |F(\mathbf{k})|$, with

$$G(\mathbf{k}) = 2t \left[2 \cos\left(\frac{\sqrt{3}}{2}k_x a\right) \cos\left(\frac{1}{2}k_x a\right) + \cos(k_y a) \right],$$

$$F(\mathbf{k}) = -\alpha \left[(1 + \sqrt{3}i) \sin\left(\frac{\sqrt{3}}{2}k_x a + \frac{1}{2}k_y a\right) + (1 - \sqrt{3}i) \sin\left(\frac{-\sqrt{3}}{2}k_x a + \frac{1}{2}k_y a\right) + 2 \sin k_y a \right]. \quad (4)$$

Here, the form factor $G(\mathbf{k})$ is coming from the nearest-neighbor hopping and $F(\mathbf{k})$ is due to the Rashba SO interaction. The chiral band energies $\varepsilon_{\tau}(\mathbf{k})$, and the wave-function

amplitudes $e_{\tau,\sigma}(\mathbf{k})$ are determined by solving the eigenvalue equation

$$\sum_{\sigma'} H_{\sigma\sigma'}(\mathbf{k}) e_{\tau,\sigma'}(\mathbf{k}) = \varepsilon_{\tau}(\mathbf{k}) e_{\tau,\sigma}(\mathbf{k}), \quad (5)$$

with $H_{\sigma\sigma'}(\mathbf{k})$ the components of the Hamiltonian (2) in Fourier space and spin basis. Its matrix form is

$$H(\mathbf{k}) = \begin{pmatrix} E_p + G(\mathbf{k}) & F(\mathbf{k}) \\ F(\mathbf{k})^* & E_p + G(\mathbf{k}) \end{pmatrix}. \quad (6)$$

The corresponding eigenvectors can be evaluated analytically,

$$e_+(\mathbf{k}) = \frac{1}{\sqrt{2}} \begin{pmatrix} 1, \frac{F(\mathbf{k})^*}{|F(\mathbf{k})|} \end{pmatrix}^T, \quad (7)$$

$$e_-(\mathbf{k}) = \frac{1}{\sqrt{2}} \begin{pmatrix} 1, -\frac{F(\mathbf{k})^*}{|F(\mathbf{k})|} \end{pmatrix}^T.$$

Then, in terms of the creation and annihilation operators for electrons in the chiral basis, H_0 becomes

$$H_0 = \sum_{\mathbf{k},\tau} \varepsilon_{\tau}(\mathbf{k}) c_{\mathbf{k},\tau}^{\dagger} c_{\mathbf{k},\tau}, \quad (8)$$

with the operators $c_{\mathbf{k},\tau}$ satisfying the canonical anticommutation relations, $\{c_{\mathbf{k},\tau}, c_{\mathbf{k}',\tau'}^{\dagger}\} = \delta(\mathbf{k} - \mathbf{k}')\delta_{\tau,\tau'}$. In this way, the surface can be described in terms of free states, but with some chiral band structure.

2. Noninteracting Green's function

In the noninteracting limit, the retarded Green's function in the real space is defined in terms of the field operators for the conduction electrons as

$$\mathcal{G}_{\sigma\sigma'}^{(0)}(\mathbf{r}_i, t; \mathbf{r}_j, t') = -i\theta(t - t') \langle \{\Psi_{\mathbf{r}_i,\sigma}(t), \Psi_{\mathbf{r}_j,\sigma'}^{\dagger}(t')\} \rangle_0, \quad (9)$$

where $\theta(t)$ is the Heaviside function. Because of the spin-orbit interaction, $\mathcal{G}_{\sigma\sigma'}^{(0)}(\mathbf{r}_i, t; \mathbf{r}_j, t')$ is diagonal in the chiral, but not in the spin space. In this context, the Fourier transformed, noninteracting retarded Green's function for the chiral band τ is $\mathcal{G}_{\tau}^{(0)}(\mathbf{k}, \omega) = [\omega - \varepsilon_{\tau}(\mathbf{k}) + i0^+]^{-1}$. Then, transforming back to the spin space one gets

$$\mathcal{G}_{\sigma\sigma'}^{(0)}(\mathbf{r}_i, \mathbf{r}_j, \omega) = \sum_{\mathbf{k},\tau} \frac{e_{\tau,\sigma}(\mathbf{k}) e_{\tau,\sigma'}^*(\mathbf{k}) e^{i\mathbf{k}(\mathbf{r}_i - \mathbf{r}_j)}}{\omega - \varepsilon_{\tau}(\mathbf{k}) + i0^+}. \quad (10)$$

This expression allows us to evaluate the density of states (DOS) for the conduction electrons as

$$\rho^{(0)}(\omega) = -\frac{1}{\pi} \text{Tr}_{\sigma} \text{Im} \mathcal{G}_{\sigma\sigma}^{(0)}(\mathbf{r}_i, \mathbf{r}_i, \omega). \quad (11)$$

In Fig. 2 we show the DOS computed by using Eq. (11) for the Au(111) surface. It displays a large van Hove feature at $\omega \approx 2.03$ eV and two sharp singularities at the band tails, see the insets in Fig. 2. The latter features are induced by the presence of the Rashba SO interaction. The van Hove singularity at high energy is due to the flattening of the upper band at the \bar{M} point,²¹ and shows up irrespective of the SO interaction. This DOS will be the input for the NRG calculations when solving the quantum impurity problem.

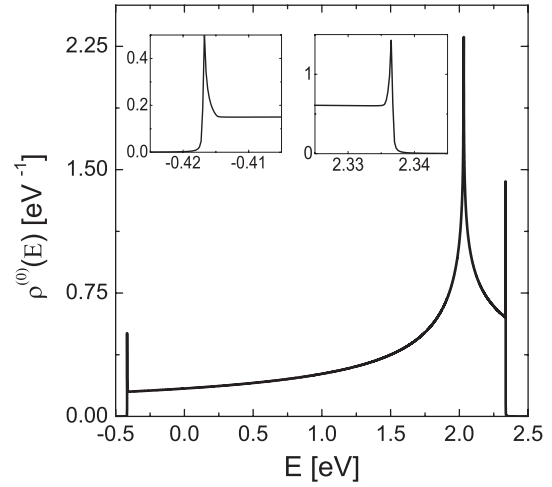


FIG. 2. The normalized DOS for the Au(111) surface obtained within the TBA. The two insets show the singularities at the band tails due to the Rashba SO interaction.

B. Modeling the quantum impurity

1. Impurity Hamiltonian

To carry out the quantitative analysis of our magnetic impurity problem, we first need to establish how the magnetic ion couples to the chiral bands. We consider here the *top configuration*, in which one Co atom is located on top of an Au atom, to which it hybridizes. The hybridization with all the other neighboring Au atoms is neglected. We have also considered other geometrical configurations (the results are not presented here), where, for example, the Co atom is placed in plane, in the middle of a hexagon, or substitutes an Au atom, hybridizing with the nearest neighbors. Despite its simplicity, the considered top configuration captures entirely the essential physics. Correspondingly, the hybridization Hamiltonian is written as

$$H_V = V \sum_{\sigma} (\Psi_{\mathbf{r}_{\text{imp}},\sigma}^{\dagger} d_{\sigma} + \text{H.c.}). \quad (12)$$

Here \mathbf{r}_{imp} labels the Au site below the Co impurity, d_{σ} annihilates an electron with spin σ at the Co orbital, and V denotes the hopping between the two orbitals. Within the NRG approach, it is convenient to model the magnetic impurity by a single local orbital which carries only a spin label. Transformed to the chiral basis, Eq. (12) becomes

$$H_V = \sum_{\tau=\pm} \sum_{\mathbf{k},\sigma} (V_{\tau,\sigma}(\mathbf{k}) c_{\mathbf{k},\tau}^{\dagger} d_{\sigma} + \text{H.c.}). \quad (13)$$

This expression is quite general, and the particular location of the impurity atom is reflected in the \mathbf{k} dependence of the hybridization factor, $V_{\tau,\sigma}(\mathbf{k})$. For the top configuration, one has $V_{\tau,\sigma}(\mathbf{k}) = V e_{\tau,\sigma}^*(\mathbf{k})$. Using Eq. (7) for the eigenvectors, one then finds $V_{\tau,\uparrow}(\mathbf{k}) = V/\sqrt{2}$ and $V_{\tau,\downarrow}(\mathbf{k}) = \tau V F(\mathbf{k})/(\sqrt{2}|F(\mathbf{k})|)$. With the hybridization Hamiltonian (13) at hand, the total Hamiltonian that describes the Co ion itself and the hybridization to the surface is

$$H = H_{\text{imp}} + H_V, \quad (14)$$

with

$$H_{\text{imp}} = \sum_{\sigma} \varepsilon_{d\sigma} d_{\sigma}^{\dagger} d_{\sigma} + U n_{\uparrow} n_{\downarrow}. \quad (15)$$

This Hamiltonian is similar to the single-impurity Anderson Hamiltonian,²² but with a somewhat modified hybridization. The first term in Eq. (15) describes the on-site energy $\varepsilon_{d\sigma} = \varepsilon_d \pm \frac{1}{2} g \mu_B B$ of the localized orbital, where we included a Zeeman splitting term due to the external magnetic field B applied along the z th direction. We assume that the g factor for the Co atom on the Au(111) surface is around $g = 2.5$. In the second term, U represents the Coulomb repulsion felt when two electrons with opposite spins occupy the orbital, with $n_{\sigma} = d_{\sigma}^{\dagger} d_{\sigma}$ denoting the occupation number. We take U and ε_d from *ab initio* calculations:³⁰ $\varepsilon_d = -0.84$ eV and $U = 2.85$ eV. The hybridization amplitude V is fixed by the Kondo temperature itself. Here, we define the Kondo temperature T_K as the half width at half maximum (HWHM) of the spectral function for the local orbital operator d_{σ} in the absence of an external magnetic field. Then, to get $T_K = 75$ K, we take $V = 0.25$ eV.

In the presence of an $SU(2)$ spin symmetry, the electrons in the spin= $\{\uparrow, \downarrow\}$ channels are scattered in the same way by the magnetic impurity. To observe any spin-resolved signal, it is necessary to break this symmetry by applying an external magnetic field along the z th direction. Then, the scattering becomes spin dependent, as the Kondo resonance is spin split.^{31,32} One drawback of such a setup is due to the large Kondo temperature:³³ a relatively large magnetic field is necessary to produce a detectable splitting of the Kondo resonance. Here we have considered $B = 3$ T.

2. Calculation of the \mathcal{T} matrix

To solve the quantum impurity problem, we employ Wilson's NRG method.²³ NRG is a powerful tool for accurate calculations of equilibrium properties of arbitrarily complex quantum impurities coupled to electron reservoirs.³⁴ The method consists in the logarithmic discretization of the continuum of conduction states, followed by a mapping to a one-dimensional chain Hamiltonian (Wilson chain) with exponentially decaying hoppings. The mapping starts with expanding the operators $c_{\mathbf{k},\tau}$ in terms of the eigenfunctions of the angular momentum,³⁵

$$c_{\mathbf{k},\tau} = \frac{1}{\sqrt{|k|}} \sum_{m=-\infty}^{\infty} \frac{1}{\sqrt{2\pi}} e^{im\phi} c_{k,\tau}^m \quad (16)$$

and then constructing an effective impurity model by integrating out the electronic angular momentum modes. The broadening felt by the impurity is given by the imaginary part of the hybridization function

$$\Delta_{\sigma}(\omega) = \sum_{\tau} \sum_{\mathbf{k}} \frac{|V_{\tau,\sigma}(\mathbf{k})|^2}{\omega - \varepsilon_{\tau}(\mathbf{k}) + i0^+}. \quad (17)$$

To a first approximation, the Rashba spin-orbit coupling is weak and does not affect the impurity spectral function $\Delta_{\uparrow}(\omega) = \Delta_{\downarrow}(\omega)$.

To determine the LMDOS, Eq. (1), one needs to calculate the full Green's function $\mathcal{G}_{\sigma\sigma'}(\mathbf{r}; \mathbf{r}; \omega)$, which can be expressed in terms of the \mathcal{T} matrix by using the Dyson equation. Let

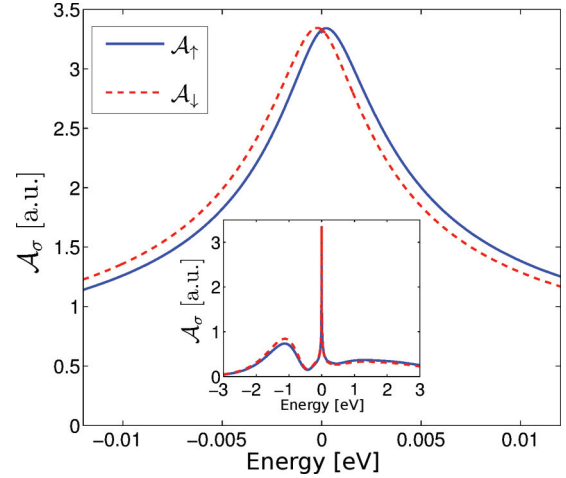


FIG. 3. (Color online) The energy dependence of the spin-dependent spectral function $\mathcal{A}_{\sigma}(\omega)$ of the local orbital around the Fermi level, calculated within the NRG approach. The splitting of the Kondo resonance is due to the external magnetic field, $B = 3$ T. The inset shows the full energy dependence of $\mathcal{A}_{\sigma}(\omega)$. The parameters for the Anderson model are $V = 0.25$ eV, $U = 2.85$ eV, and $\varepsilon_d = -0.84$ eV.

us now focus on the calculation of the \mathcal{T} matrix itself. For quantum impurity models, one of the most elegant ways to perform this task is to relate it to some local correlation function that can be computed numerically with the NRG. For the Anderson model, the \mathcal{T} matrix is related to the Green's function of the d_{σ} operators.^{36,37} For a constant and real coupling V , the imaginary and real parts of the spin-resolved \mathcal{T} matrix are then given by

$$\begin{aligned} \text{Im}\mathcal{T}_{\sigma}(\omega) &= -\pi V^2 \mathcal{A}_{\sigma}(\omega), \\ \text{Re}\mathcal{T}_{\sigma}(\omega) &= V^2 \mathcal{P} \int d\omega' \frac{\mathcal{A}_{\sigma}(\omega')}{\omega - \omega'}, \end{aligned} \quad (18)$$

with $\mathcal{A}_{\sigma}(\omega)$ the spectral function of the d_{σ} operators and \mathcal{P} denoting a principal value integral. To obtain reliable results for the spin-dependent spectral functions, we have employed the density-matrix NRG.³⁸ In addition, we have included in our calculations the full energy dependence of $\varrho^{(0)}(E)$ for the Au(111) surface.

In Fig. 3 we show the energy dependence of the spin-resolved spectral function $\mathcal{A}_{\sigma}(\omega)$ in the vicinity of the Fermi level, with the inset presenting its full energy dependence. Although $\varrho^{(0)}(E)$ shows a gap below $E < -0.42$ eV (the bandwidth in the NRG calculations was fixed to $D = 2.5$ eV), the two Hubbard satellites and the Kondo peak at the Fermi level are clearly visible. The splitting of the Kondo resonance for $B = 3$ T is visible in $\mathcal{A}_{\sigma}(\omega)$. Within our model $\Gamma = \pi V^2 \varrho(0) \gg T_K \gg \Delta E_Z^{\text{imp}}$, with ΔE_Z^{imp} the Zeeman splitting. The applied magnetic field is not strong enough to suppress the Kondo resonance, however, it is sufficient to produce a spin-resolved response detectable in the LMDOS. The $\mathcal{A}_{\sigma}(\omega)$ in Fig. 3 was computed at $T = 0$, but it can be argued that our findings remain valid as long as we are in the Kondo regime: $T < \min\{T_K, B\}$. If the temperature increases, the Kondo peak becomes suppressed and eventually, at high

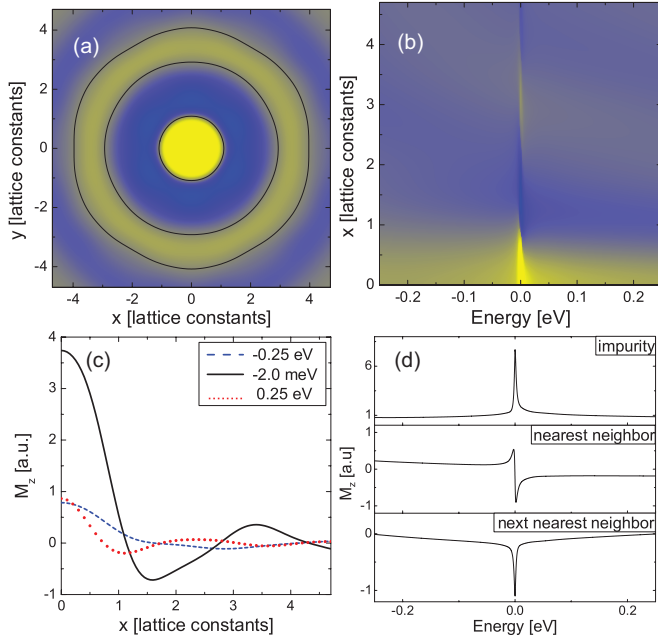


FIG. 4. (Color online) (a) The spatial distribution of the z th component of the LMDOS, M_z , around the Kondo impurity at energy $E = -2$ meV, below E_F and (c) the corresponding cuts at different energies. The impurity is located at the center. The pattern formed around the magnetic impurity has a hexagonal symmetry and exhibits oscillations with distance from the impurity, with a period depending on the energy. The bright (dark) color corresponds to maximum (minimum) value of M_z . (b) M_z as a function of energy and distance from the impurity along the x direction, and (d) the energy dependence of $M_z(E)$ calculated at the impurity site and the two nearest-neighbor sites.

temperatures $T \gg T_K$, it is completely smeared out by thermal fluctuations.

III. LMDOS: ANALYSIS OF THE NUMERICAL RESULTS

In this section we shall describe how we compute the LMDOS. As discussed in Sec. I, the LMDOS can be related to the single-particle Green's function, see Eq. (1), and satisfies the Dyson equation, when expressed in terms of the \mathcal{T} matrix. While this expression is somewhat cumbersome in the chiral basis due to the presence of different form factors, in the spin space it simplifies considerably:

$$\begin{aligned} \mathcal{G}_{\sigma\sigma'}(\mathbf{r}, \mathbf{r}', \omega) &= \mathcal{G}_{\sigma\sigma'}^{(0)}(\mathbf{r}, \mathbf{r}', \omega) + \sum_{\sigma''} \mathcal{G}_{\sigma\sigma''}^{(0)}(\mathbf{r}, \mathbf{r}_{\text{imp}}, \omega) \\ &\quad \times \mathcal{T}_{\sigma''}(\mathbf{r}_{\text{imp}}, \omega) \mathcal{G}_{\sigma''\sigma'}^{(0)}(\mathbf{r}_{\text{imp}}, \mathbf{r}', \omega). \end{aligned} \quad (19)$$

The LMDOS can be calculated from $\delta \mathcal{G}_{\sigma\sigma'}(\mathbf{r}, \mathbf{r}, \omega) = \mathcal{G}_{\sigma\sigma'}(\mathbf{r}, \mathbf{r}, \omega) - \mathcal{G}_{\sigma\sigma'}^{(0)}(\mathbf{r}, \mathbf{r}, \omega)$, by replacing $\mathcal{G}(\mathbf{r}, \mathbf{r}, \omega) \rightarrow \delta \mathcal{G}(\mathbf{r}, \mathbf{r}, \omega)$ in Eq. (1). Notice that the spin impurity acts as a simple point scatterer, and that in the magnetic response, only the second term in Eq. (19) gives a finite contribution.

Within the present formalism, we are able to analyze both the spatial and the energy dependence of the local magnetization components. Here we will focus on \mathbf{M}_r and the out-of-plane, M_z component of the LMDOS. The spatial distribution of the M_z , calculated at energy $E = -2$ meV,

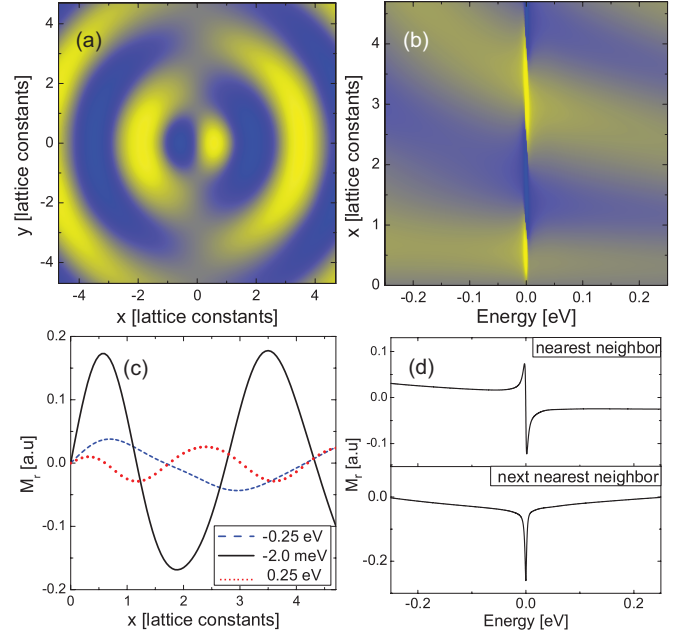


FIG. 5. (Color online) (a) The spatial distribution of the in-plane x component of the LMDOS, M_x , around the Kondo impurity at energy $E = -2$ meV, and (c) the corresponding cuts (in the x direction) at different energies. (b) M_r as a function of energy and distance from the impurity along the x direction, and (d) the energy dependence of $M_r(\omega)$ calculated at the nearest and next-nearest neighbor sites.

is displayed in Fig. 4(a). The bright (dark) areas correspond to the maxima (minima) of M_z . One can see that its spatial dependence displays a hexagonal symmetry with respect to the position of the magnetic impurity. Moreover, M_z exhibits oscillations with an energy-dependent period. This behavior is displayed in Fig. 4(c). When moving away from the Fermi energy, the magnitude of M_z decreases and the period of the oscillations becomes shorter as the energy is increased from negative to positive values. This is presented in Fig. 4(b), which explicitly shows the energy and spatial dependence of M_z when E is swept across the Fermi surface. Close to E_F , the asymmetry induced by B in the spin sector, together with the presence of the split Kondo resonance, maximizes the amplitude of the local magnetization. However, when the energy is detuned from E_F , the LMDOS becomes suddenly suppressed, leading to a Fano-like resonance, similar to the LDOS.³⁹ Moreover, the shape and magnitude of such a Fano resonance changes as one moves away from the impurity site, see Fig. 4(d). One should note that within the TBA, although we have represented the spatial distributions as continuous, the calculations are only valid at the atomic sites.

In a finite B , the features observed in M_z are present irrespective of the presence of the Rashba SO interaction at the surface. On the other hand, M_r is very sensitive to the Rashba effect. Finite α implies $M_r \neq 0$, otherwise M_r vanishes. The spatial distribution of M_r around the magnetic impurity together with its energy dependence are presented in Fig. 5. First of all, one can note that in the vicinity of magnetic impurity, the amplitude of M_r is smaller by approximately one order of magnitude than the amplitude of M_z . In fact, M_r

vanishes exactly at the impurity site, while M_z has a maximum there, see, for example, Figs. 4(a), 4(c), 5(a) and 5(c). However, with increasing distance from the impurity, $x > 3-4a$, both M_r and M_z become comparable and, in fact, for larger distances, the radial component can overtake M_z , as its decay is much slower than that of the z th component. The basic properties of the spatial dependence of M_r can be deduced from Fig. 5(a). One can see that M_r is an odd function with respect to the radial distance, and oscillates with approximately the same period as M_z . Again, the highest amplitude of M_r occurs for energies around the Fermi energy due to the Kondo effect, and as the energy increases, the period of the oscillations decreases, see Figs. 5(b) and 5(c). The spatial and energy dependence of M_r is shown in Fig. 5(b), while M_r at some particular positions is displayed in Fig. 5(d). It can be seen that the shape of the resonance at the nearest-neighbor and the second-nearest-neighbor sites is similar to that of M_z [cf. Fig. 4(d)]. These results around the Fermi energy are robust with respect to the parameters of our model, the only determining parameter being T_K .

Finally, we would like to emphasize that M_r is, on one hand, proportional to the strength of the SO interaction, and on the other hand, to the asymmetry of the \mathcal{T} -matrix components for the spin- \uparrow and spin- \downarrow channels. While α is an intrinsic feature of the surface, the asymmetry between the spin- \uparrow and spin- \downarrow channels can be changed by simply applying an external magnetic field. This guarantees that the topographic map of the surface develops interference patterns in M_r if the Rashba interaction is present. Therefore, the measurement of the in-plane component of the LMDOS offers an alternative way to angle-resolved photoemission spectroscopy (ARPES)⁴ to identify surfaces with spin-orbit interaction.

IV. CONCLUDING REMARKS

In the present work we have investigated the behavior of the local magnetization density of states around a magnetic impurity in the Kondo regime, coupled to a metallic surface with Rashba spin-orbit interaction. To make realistic estimates, we have considered a Co impurity on top of a Au(111) surface. This problem has been addressed using band structure calculations and the NRG method, which allowed us to obtain reliable predictions for the LMDOS.

In particular, we have studied the spatial and energy dependence of the LMDOS for both the radial (in-plane) and z th (out-of-plane) components. We have found that the in-plane component of the LMDOS is a pure Rashba effect. Furthermore, it turned out that the radial component displays oscillations with the distance from the impurity, and decays much slower than the z th component, so that at larger distances, the in-plane component may become dominant. Since M_r vanishes in the absence of spin-orbit interaction, measuring the radial component using spin-polarized STM, provides a way to confirm/infirm the presence of the Rashba effect on surfaces. Our observations provide thus an alternative route to investigate the spin splitting of any surface states, first observed by angle-resolved photoemission spectroscopy⁴ in Au(111).

ACKNOWLEDGMENTS

This research has been supported by financial support from UEFISCDI under French-Romanian Grant DYMESYS (ANR 2011-IS04-001-01 and Contract No. PN-II-ID-JRP-2011-1). I.W. acknowledges support from the ‘‘Luventus Plus’’ Project No. IP2011 059471 for the years 2012–2014, and the EU Grant No. CIG-303 689.

*chirlarazvan@yahoo.com

¹R. Winkler, *Spin-Orbit Coupling Effects in Two-Dimensional Electron and Hole Systems* (Springer, New York, 2003).

²E. I. Rashba, *Sov. Phys. Solid State* **2**, 1109 (1960).

³D. Awschalom and N. Samarth, *Physics* **2**, 50 (2009).

⁴S. LaShell, B. A. McDougall, and E. Jensen, *Phys. Rev. Lett.* **77**, 3419 (1996).

⁵L. Petersen and P. Hedegard, *Surf. Sci.* **459**, 49 (2000).

⁶J. D. Walls and E. J. Heller, *Nano Lett.* **7**, 3377 (2007).

⁷A. T. Ngo, J. Rodriguez-Laguna, S. E. Ulloa, and E. H. Kim, *Nano Lett.* **12**, 13 (2012).

⁸S. Becker, M. Liebmann, T. Mashoff, M. Pratzner, and M. Morgenstern, *Phys. Rev. B* **81**, 155308 (2010).

⁹M. R. Galpin, F. W. Jayatilaka, D. E. Logan, and F. B. Anders, *Phys. Rev. B* **81**, 075437 (2010).

¹⁰S. Lounis, A. Bringer, and S. Blügel, *Phys. Rev. Lett.* **108**, 207202 (2012).

¹¹J. Kondo, *Prog. Theor. Phys.* **32**, 37 (1964).

¹²A. C. Hewson, *The Kondo Problem to Heavy Fermions* (Cambridge University Press, Cambridge, England, 1993).

¹³Y. Meir and N. S. Wingreen, *Phys. Rev. B* **50**, 4947 (1994).

¹⁴J. Malecki, *J. Stat. Phys.* **129**, 741 (2007).

¹⁵R. Žitko and J. Bonča, *Phys. Rev. B* **84**, 193411 (2011).

¹⁶M. Zarea, S. E. Ulloa, and N. Sandler, *Phys. Rev. Lett.* **108**, 046601 (2012).

¹⁷T. Yanagisawa, *J. Phys. Soc. Jpn.* **81**, 094713 (2012).

¹⁸L. Isaev, D. F. Agterberg, and I. Vekhter, *Phys. Rev. B* **85**, 081107 (2012).

¹⁹V. Madhavan, W. Chen, T. Jamneala, M. F. Crommie, and N. S. Wingreen, *Science* **280**, 567 (1998).

²⁰V. Madhavan, W. Chen, T. Jamneala, M. F. Crommie, and N. S. Wingreen, *Phys. Rev. B* **64**, 165412 (2001).

²¹M.-H. Liu, S.-H. Chen, and C.-R. Chang, *Phys. Rev. B* **78**, 195413 (2008).

²²P. W. Anderson, *Phys. Rev.* **124**, 41 (1961).

²³K. G. Wilson, *Rev. Mod. Phys.* **47**, 773 (1975).

²⁴N. Knorr, M. A. Schneider, L. Diekhöner, P. Wahl, and K. Kern, *Phys. Rev. Lett.* **88**, 096804 (2002).

²⁵M. Schneider, L. Vitali, P. Wahl, N. Knorr, L. Diekhauer, G. Wittich, M. Vogelgesang, and K. Kern, *Appl. Phys. A* **80**, 937 (2005).

²⁶G. A. Fiete and E. J. Heller, *Rev. Mod. Phys.* **75**, 933 (2003).

²⁷R. Wiesendanger, *Rev. Mod. Phys.* **81**, 1495 (2009).

²⁸W. Chen, V. Madhavan, T. Jamneala, and M. F. Crommie, *Phys. Rev. Lett.* **80**, 1469 (1998).

²⁹N. Takeuchi, C. T. Chan, and K. M. Ho, *Phys. Rev. B* **43**, 13899 (1991).

- ³⁰O. Újsághy, J. Kroha, L. Szunyogh, and A. Zawadowski, *Phys. Rev. Lett.* **85**, 2557 (2000).
- ³¹T. A. Costi, *Phys. Rev. Lett.* **85**, 1504 (2000).
- ³²A. V. Kretinin, H. Shtrikman, D. Goldhaber-Gordon, M. Hanl, A. Weichselbaum, J. von Delft, T. Costi, and D. Mahalu, *Phys. Rev. B* **84**, 245316 (2011).
- ³³W. Wei, R. Rosenbaum, and G. Bergmann, *Phys. Rev. B* **39**, 4568 (1989).
- ³⁴R. Bulla, T. A. Costi, and T. Pruschke, *Rev. Mod. Phys.* **80**, 395 (2008).
- ³⁵H. R. Krishna-murthy, J. W. Wilkins, and K. G. Wilson, *Phys. Rev. B* **21**, 1003 (1980).
- ³⁶D. C. Langreth, *Phys. Rev.* **150**, 516 (1966).
- ³⁷L. Borda, L. Fritz, N. Andrei, and G. Zaránd, *Phys. Rev. B* **75**, 235112 (2007).
- ³⁸We used the open-access Budapest Flexible DM-NRG code, <http://www.phy.bme.hu/~dmnrg/>; O. Legeza, C. P. Moca, A. I. Tóth, I. Weymann, and G. Zaránd, *arXiv:0809.3143*.
- ³⁹A. E. Miroshnichenko, S. Flach, and Y. S. Kivshar, *Rev. Mod. Phys.* **82**, 2257 (2010).